Supporting information for

Synergistic effects at the interface of core-shell Cu_3P@CoO heterojunctions for enhanced nitrate reduction to ammonia

Jiujiang Xian,[a] Yushu Gou,[b] Manduo Huang,[a] Yuanming Mu,[a] Shilin Zhang,[a] Yuyao Ji,[a*]

[a]College of Chemistry and Materials Science, Sichuan Normal University, Chengdu 610068, Sichuan, China.

[b]School of Healthcare Technology, Chengdu Neusoft University, 611844, Sichuan, China

[*] E-mail: yyji@sicnu.edu.cn;

Content

Experimental Section

Preparation of Cu_3P nanowire array catalyst: A precursor solution was prepared by dissolving 0.6 g of NaOH and 0.15 g of $(NH_4)_2S_2O_8$ in 20 mL of deionized water. This solution was sealed within a Teflon-lined autoclave for hydrothermal treatment at 60–80 °C over a period of 2 h. The resulting intermediates were subsequently converted to phosphides via a vapor-phase reaction using NaH_2PO_2 as the phosphorus source. Specifically, the samples were annealed under an inert atmosphere, ramping from room temperature to 300–350 °C at 2–5 °C min^{-1} and holding for 2 hours to allow PH_3 generation and diffusion. Upon cooling, the final products underwent a brief rinse with deionized water to remove surface residues before being dried under vacuum.

Preparation of Cu_3P@CoO core–shell heterostructure catalyst: 1.09 g $Co(NO_3)_2 \cdot 6H_2O$ and 1.04 g urea were mixed in 50 mL water with stirring. Then, the solution together with Cu_3P/CF was transferred into a Teflon-lined autoclave for the hydrothermal reaction at 120 °C. After washing and drying, the samples were subjected to annealing at 300 °C under Ar atmosphere for 2 h.

Electrochemical measurements: N_2 reduction experiments were carried out in atwo-compartment cell under ambient condition, which was separated by Nafion 117 membrane. The membrane was protonated by first boiling in ultrapure water for 1 hand treating in H_2O_2 (5 wt%) aqueous solution at 80 °C for another 1 h, respectively. And then, the membrane was treaded in 0.5 M H_2SO_4 for 3 h at 80 °C and finally in water for 6 h. The electrochemical experiments were carried out with an electrochemical workstation (CHI 660E) using a three-electrode configuration with prepared electrodes, graphite rod and Ag/AgCl electrode (saturated KCl electrolyte) as working electrode, counter electrode and reference electrode, respectively. The potentials reported in this work were converted to reversible hydrogen electrode (RHE) scale via calibration with the following equation: E (vs. RHE) = E (vs.Ag/AgCl) + 0.059 × pH + 0.197 V and the

presented current density was normalized to the geometric surface area. For electrochemical N_2 reduction, chrono-amperometry tests were conducted in N_2-saturated 1.0 M Na_2SO_4 solution.

Determination of NH_3: All the electrochemical measurements were investigated in an H-shape reactor separated by a treated Nafion 117 membrane by using the CHI660E electrochemical workstation (Chenhua, Shanghai) with a standard three-electrode setup (Cu_3P@CoO (1 × 0.5 cm^2) as the working electrode, a carbon rod as the counter electrode, and a Ag/AgCl as the reference electrode. All the potentials reported in our work were converted to reversible hydrogen electrode (RHE) scale via calibration with the following equation: E (RHE) = E (vs. Ag/AgCl) + 0.0591 × pH + 0.197 V and the current density was normalized by the geometric surface area. The concentration of produced NH_3 was determined by spectrophotometry measurement with the indophenol blue method.[1] The indophenol blue method is employed by Bethelot reaction queation.[2,3] The ammonia reacts with phenol and hypochlorite in alkaline solution. The generated indophenol product is in blue color. The obtained electrolyte was firstly diluted 50 times, for further test. In detail, 2 mL of the diluted catholyte was obtained from the cathodic chamber and mixed with 2 mL of the 1 M NaOH solution that contained 5% salicylic acid and 5% sodium citrate. Then, 1 mL of 0.05 M NaClO and 0.2 mL of 1 wt% $C_5FeN_6Na_2O$ were dropped into the collected electrolyte solution. After standing at room temperature for 2 h, the ultraviolet-visible absorption spectrum was measured. The concentration-absorbance curve was calibrated using the standard NH_4Cl solution with NH_3 concentrations in 0.1 M NaOH. The absorbance at 655 nm was measured to quantify the NH_3 concentration.

Determination of NO_2^-: The NO_2^- concentration was analyzed using the Griess test.[4] The Griess reagent was prepared by dissolving 0.1 g N-(1-naphthyl) ethylenediamine dihydrochloride, 1.0 g sulfonamide, and 2.94 mL H_3PO_4 in 50 mL deionized water. In a typical colorimetric assay, the 1.0 mL Griess reagent was

mixed with the 1.0 mL nitrite-containing solution and 2.0 mL H_2O and allowed to react at room temperature for 10 mins, in which sulfonamide reacts with NO_2^- to form a diazonium salt and then further reacts with the amine to form an azo dye (magenta). The absorbance at 540 nm was measured to quantify the NO_2^- concentration.

Determination of N_2H_4: In this work, we used the method of Watt and Chrisp[5] to determine the concentration of produced N_2H_4. The chromogenic reagent was a mixed solution of 5.99 g $C_9H_{11}NO$, 30 mL HCl and 300 mL C_2H_5OH. In detail, 1 mL electrolyte was added into 1 mL prepared color reagent and stirred for 15 min in the dark. The absorbance at 455 nm was measured to quantify the N_2H_4 concentration.

Computational Details: Spin-polarized density functional theory (DFT) method was employed in all computations.[6,7] The structural model of the Cu_3P@CoO heterojunction was designed to match our HRTEM observations, specifically aligning the Cu_3P (112) and CoO (200) planes. Our slab models included atomic layers with Å vacuum gap. We fixed the bottom layers to simulate bulk constraints and relaxed the remaining atoms and adsorbates until the force threshold reached 0.02 eV/Å. A comprehensive search involving top, bridge, and hollow sites on both single components and the interface revealed that NO_3^- adsorption is energetically most favorable at the heterojunction. Here, the Co sites become highly active due to the synergistic electron flow originating from the Cu_3P support. The core electrons were described using the projector- augmented-wave (PAW) method, while the Perdew–Burke–Ernzehof (PBE) functional with in the generalized gradient approximation (GGA) was utilized to treat the electronic exchange-correlation energy.[8] The spin polarization was adopted and its influence on the energy minima were also considered for all calculations.[9] All atomic structures were optimized until the energy and force reached the convergence thresholds of 10^{-4} eV and -0.02 eV/ Å, respectively. The energy cutoff was set to 450 eV. A Monkhorst-Pack k-mesh with a 4 × 4 × 1 k-point grid was used for

structural optimization and frequency calculations, while 6 × 6 × 1 k-point grid was utilized for electronic structure calculations. The Gibbs free energy change (ΔG) involved in each elementary reaction calculation was calculated based on terms of the computational hydrogen electrode model proposed by Nørskov et al.[10,11] The calculation formula is: $\Delta G=\Delta E + \Delta ZPE - T\Delta S + eU + \Delta GpH$. Here, ΔE is the DFT-calculated total energy, T is set to 298.15 K and the entropy S is computed by fixing the catalyst base as the premise. U is the electrode potential versus reversible hydrogen electrode (RHE). ΔGpH represents the correction of the free energy because of the variations in pH conditions. ΔGmax represents the maximum ΔG among each elementary reaction.

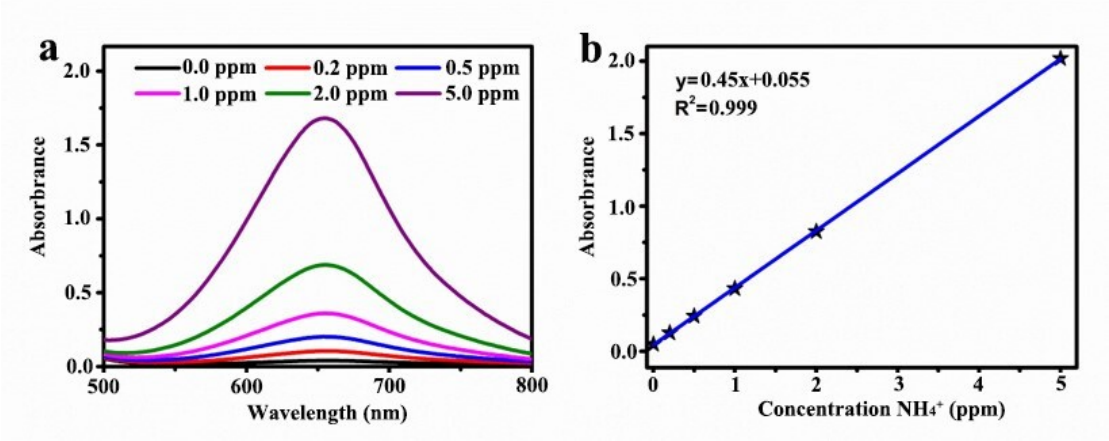

Fig. S1. UV-Vis absorption spectra of a) indophenol assays kept with different concentrations of NH_4^+ after incubated for 2 h at room temperature. Calibration curve used for estimation of b) NH_4^+ concentration.

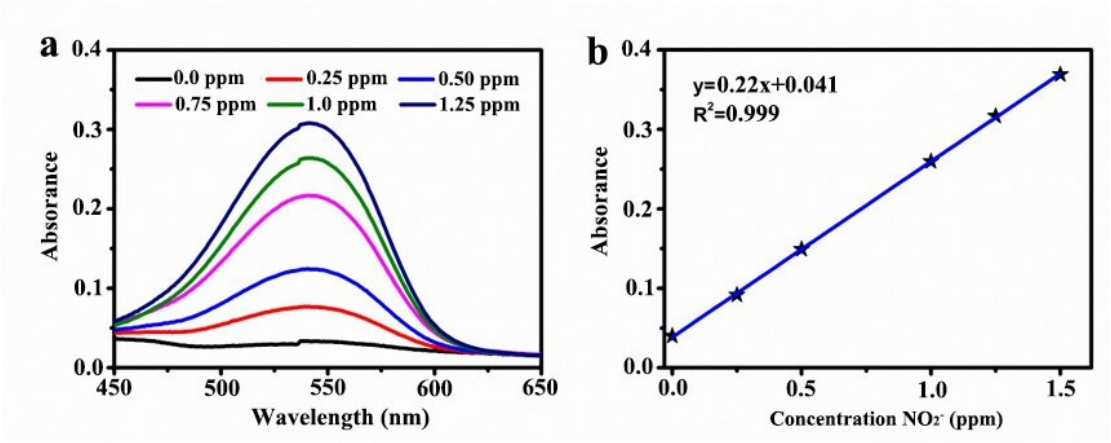

Fig. S2. UV-Vis absorption spectra of a) various NO_2^- concentrations after incubated for 10 mins at room temperature. Calibration curve used for quantification of b) NO_2^- concentration.

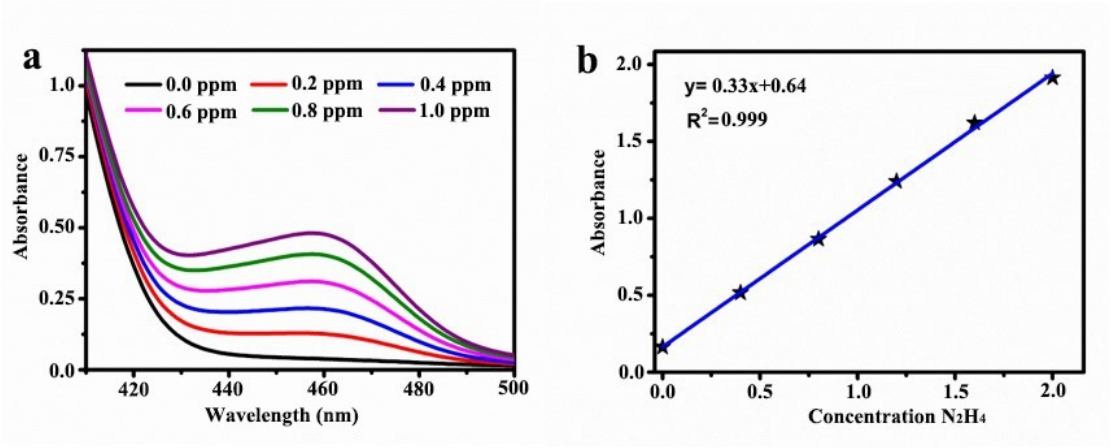

Fig. S3. UV-vis absorption spectra of a) indophenol assays with NH_3 concentrations after incubated for 1 h at room temperature. Calibration curve used for estimation of b) NH_3 concentration.

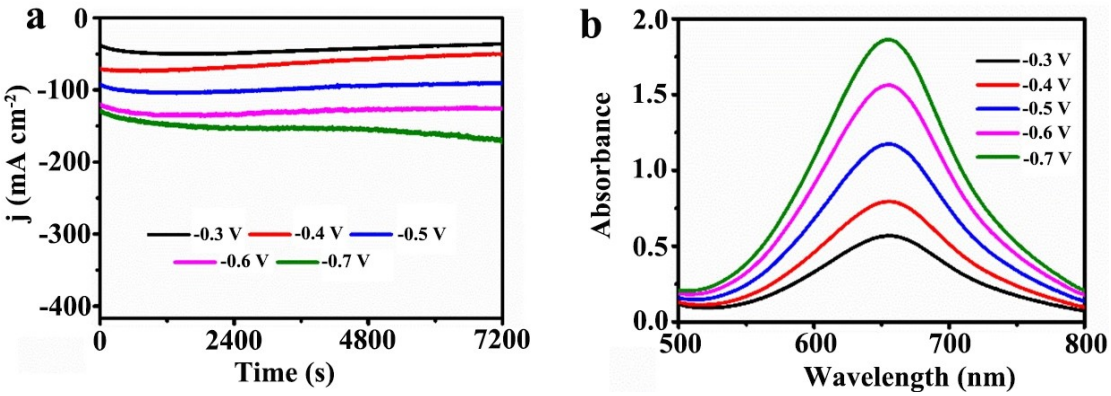

Fig. S4. Chronoamperometry curves of a) Cu_3P@CoO at different given potentials. b) UV-Vis absorption spectra.

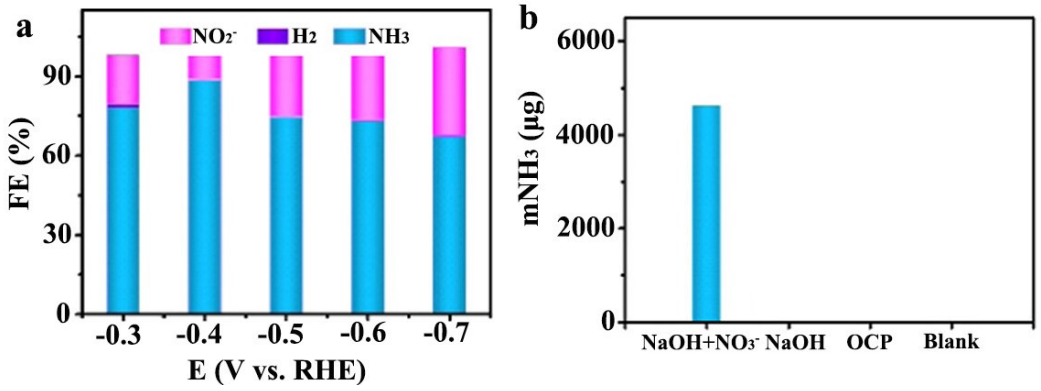

Fig. S5. Product distribution of a) Cu_3P@CoO. NO_3^-RR performance of b) Cu_3P@CoO under different test conditions.

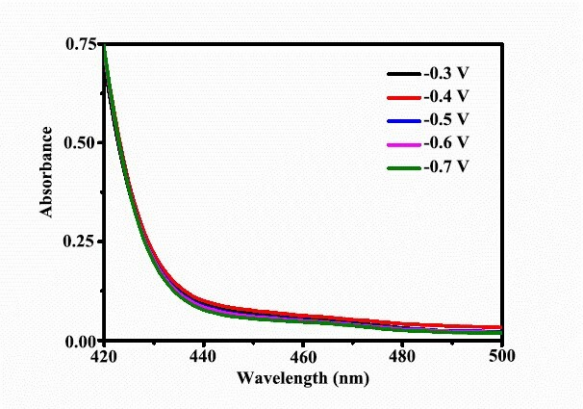

Fig. S6. UV-Vis absorption spectra of the electrolytes estimated by the method of Watt and Chrisp before and after 3-h electrolysis at room temperature.

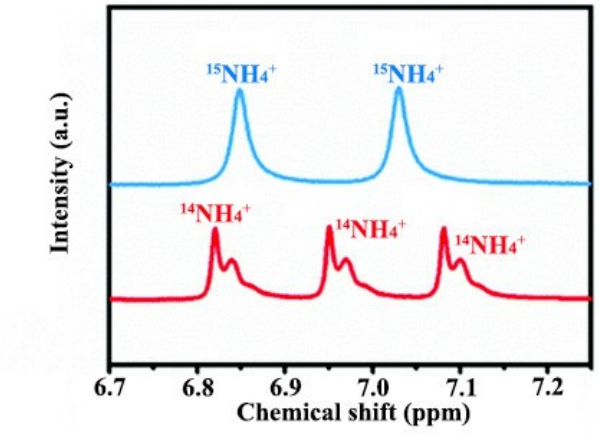

Fig. S7. ^{1}H NMR spectra of standard samples.

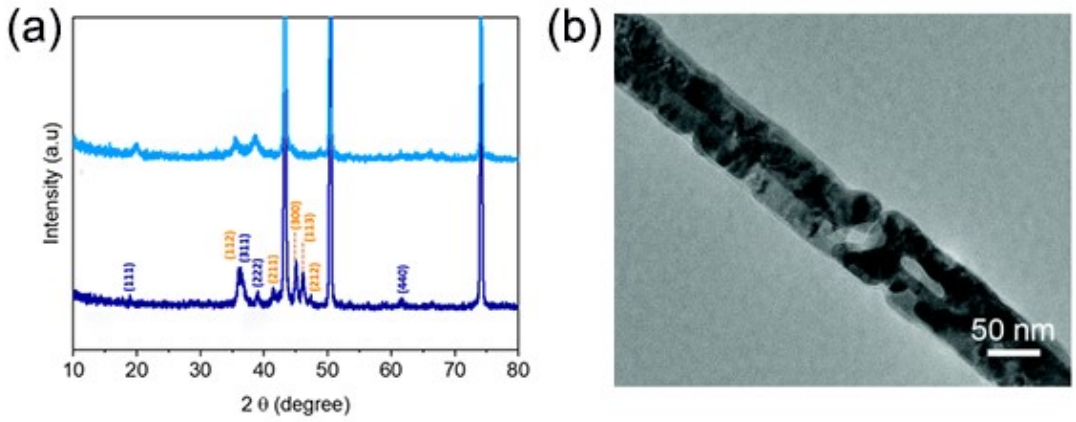

Fig. S8. (a) XRD and (b) TEM images of Cu_3P@CoO after long time test.

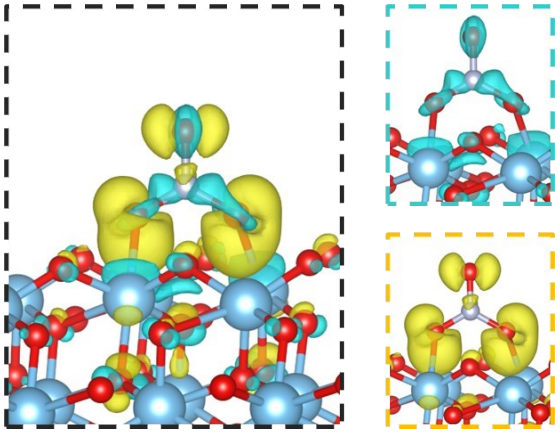

Fig. S9. Charge density difference of CoO with adsorbed NO_3^-.

Table S1. Comparison of the electrocatalytic NO_3RR performances of Cu_3P@CoO catalysts with other extensively reported electrocatalysts.

Electrocatalyst	Electrolyte	FE(%)	NH_3 Yield rate ($mg\ h^{-1}mg_{cat}^{-1}$)	Ref.
TiO_{2-X}	0.1 M K_2SO_4 + 0.5 M KNO_3	85	0.765	[10]
Cu/Cu_2O	0.5 M Na_2SO_4 + 200 ppm NO_3^--N	95.8	4.16	[11]
$Ir\&Cu/Cu_2O$	1M KOH + 0.1M KNO_3	92	8.228	[12]
v_{Co}-Co_3O_4/CC	0.1 M NaOH + 0.1M KNO_3	97.2	8.7975	[13]
xRu/Co_3O_4	0.1 M KOH + 0.1 M KNO_3	75.7	0.01598	[14]
Co/CoO	0.1 M Na_2SO_4 + 200 ppm NO_3^--N	93.8	3.31	[15]
Fe single atom	0.1 M K_2SO_4 + 0.5 M KNO_3	75	5.2	[16]
$Cu_{49}Fe_1$	0.1 M K_2SO_4 + 200 ppm KNO_3	94.5	0.046	[17]

$Cu–WO_3$	0.1 M KOH + 0.1 M KNO_3	94%	2.13	[18]
$CoMoO_4$	0.5 M Na_2SO_4 + 0.1 M KNO_3	91.17%	1.48	[19]
Bi/Cu_2O	0.5 M Na_2SO_4 + 0.1 M $NaNO_3$	99.2%	2.56	[20]
Cu_1Co_1-BCN	0.1 M KOH + 0.1 M KNO_3	92.44%	6.41	[21]
Co_3O_4/Cu	0.05 M Na_2SO_4 + 0.1 M $NaNO_3$	94.6%	0.684	[22]
Fe-Co_3O_4	0.5 M Na_2SO_4 + 0.1 M KNO_3	95.5%	0.624	[23]

References

[1] D. Zhu, L. Zhang, R. E. Ruther, R. J. Hamers, Photo-illuminated diamond as a solid-state source of solvated electrons in water for nitrogen reduction. *Nat. Mater.*, 2013, **12**, 836-841.

[2] Y. Zhao, R. Shi, X. Bian, C. Zhou, Y. Zhao, S. Zhang, F. Wu, G. I. N. Waterhouse, L. Z. Wu, C. H. Tung, T. Zhang, Ammonia detection methods in photocatalytic and electrocatalytic experiments: How to improve the reliability of NH_3 production rates?. *Adv. Sci.*, 2019, **6**, 1802109.

[3] D. Yao, C. Tang, L. Li, B. Xia, A. Vasileff, H. Jin, Y. Zhang, S. Z. Qiao, In situ fragmented bismuth nanoparticles for electrocatalytic nitrogen reduction. *Adv. Energy Mater.*, 2020, **10**, 2001289.

[4] G. W. Watt, J. D. Chrisp, Spectrophotometric method for determination of hydrazine. *Anal. Chem.*, 1952, **24**, 2006-2008.

[5] G. Kresse, J. Hafner, Ab initio molecular-dynamics simulation of the liquid-metal–amorphous-semiconductor transition in germanium. *Phys. Rev. B,* 1994, **49**, 14251-14269.

[6] Q. Zhou, F. Gong, Y. Xie, R. Xiao, 1+1>2: Learning from the interfacial modulation on single-atom electrocatalysts to design dual-atom electrocatalysts for dinitrogen reduction. *Green Energy Environ.,* 2023, **8**, 139-149.

[7] Q. Zhou, F. Gong, Y. Xie, D. Xia, Z. Hu, S. Wang, L. Liu, R. Xiao, A general strategy for designing metal-free catalysts for highly-efficient nitric oxide reduction to ammonia. *Fuel*, 2022, **310**, 122442.

[8] B. Wang, T. Li, F. Gong, M. H. D. Othman, R. Xiao, Ammonia as a green energy carrier: Electrochemical synthesis and direct ammonia fuel Eell-a comprehensive review. *Fuel Process. Technol.*, 2022, **235**, 107380.

[9] X. Sun, F. Gong, M. Hao, L. Wu, C. Yin, Z. Sun, R. Xiao, Enhanced thermal transport and corrosion resistance by coating vertically-aligned graphene on zirconium alloy for nuclear reactor applications. *Appl. Surf. Sci.*, 2022, **582**, 152484.

[10] R. Jia, Y. Wang, C. Wang, Y. Ling, Y. Yu, B. Zhang, Boosting Selective Nitrate Electroreduction to Ammonium by Constructing Oxygen Vacancies in TiO_2. *ACS Catal.,* 2020, **10**, 3533-3540.

[11] Y. Wang, W. Zhou, R. Jia, Y. Yu, B. Zhang, Unveiling the activity origin of a copper-based electrocatalyst for selective nitrate reduction to ammonia. *Angew. Chem. Int. Ed.*, 2020, **59**, 5350.

[12] M. A. Akram, B. Zhu, J. Cai, S. Qin, X. Hou, P. Jin, F. Wang, Y. He, X. Li, L. Feng, Hierarchical nanospheres with polycrystalline Ir&Cu and amorphous Cu_2O toward energy-efficient nitrate electrolysis to ammonia. *Small*, 2023, **19**, e2206966.

[13] Z. Deng, C. Ma, Z. Li, Y. Luo, L. Zhang, S. Sun, Q. Liu, J. Du, Q. Lu, B. Zheng, X. Sun, High-efficiency electrochemical nitrate reduction to ammonia on a Co_3O_4 nanoarray catalyst with cobalt vacancies. *ACS Appl. Mater. Interfaces*, 2022, **14**, 46595–46602.

[14] Y. Yu, C. Wang, Y. Yu, Y. Wang, B. Zhang, Promoting selective electroreduction of nitrates to ammonia over electron-deficient Co modulated by rectifying schottky contacts. *Sci. China: Chem.*, 2020, **63**, 1469.

[15] C. Wang, Z. Liu, T. Hu, J. Li, L. Dong, F. Du, C. Li, C. Guo, Metasequoia-like nanocrystal of iron-doped copper for efficient electrocatalytic nitrate reduction into ammonia in neutral media. *ChemSusChem.*, 2021, **14**, 1825-1829.

[16] T. Zhu, Q. Chen, P. Liao, W. Duan, S. Liang, Z. Yan, C. Feng, Single-atom Cu catalysts for enhanced electrocatalytic nitrate reduction with significant alleviation of nitrite production. *Small*, 2020, **16**, e2004526.

[17] X. Zhang, C. Wang, Y. Guo, B. Zhang, Y. Wang, Y. Yu, Cu clusters/TiO_{2-x} with abundant oxygen vacancies for enhanced electrocatalytic nitrate reduction to ammonia. *J. Mater. Chem. A*, 2022, **10**, 6448.

[18] M. Wu, S. Li, K. Wei, H. Hu, Y. Song, Z. Zheng, H. Li, F. Gao, Structural optimization of oxygen vacancies in WO_3 via Cu doping for enhanced electrocatalytic nitrate reduction to ammonia. *Inorg. Chem. Front.*, 2025, **12**, 6631-6639.

[19] Y. Xu, L. Cao, H. Hua, R. Li, Y. Wang, J. Liu, Y. Wang, C. Fan, Electrocatalytic reduction of nitrate to ammonia on $CoMoO_4$ microspheres: A comparative study with Co_3O_4. *Chem. Eng. J.*, 2025, **508**, 160985.

[20] T. K. C. Phu, W. T. Hong, H. Han, Y. I. Song, J. H. Kim, S. H. Roh, M. C. Kim, J. H. Koh, B. K. Oh, J. Y. Kim, C. H. Chung, D. H. Lee, J. K. Kim, Conformal surface intensive doping of low-valence Bi on Cu_2O for highly efficient electrochemical nitrate reduction to ammonia production. *Mater. Today*, 2024, **76**, 1369-7021.

[21] J. Wang, Z. Fan, H. Zhao, H. Liu, M. Zheng, L. Zhang, Y. Zhou, L. Sun, J. Liu, H. Zhang, High faraday efficiency of Cu_1Co_1-BCN based on a dodecahydro-closo-dodecaborate hybrid for electrocatalytic reduction of nitrate to ammonia. *J. Mater. Chem. A*, 2023, **11**, 20234-20241.

[22] W. Fu, Z. Hu, Y. Du, P. Su, Y. Su, Q. Zhang, M. Zhou, Building dual active sites Co_3O_4/Cu electrode to break scaling relations for enhancement of electrochemical reduction of nitrate to high-value ammonia. *J. Hazard. Mater.*, 2022, **434**, 128887.

[23] P. Wei, J. Liang, Q. Liu, L. Xie, X. Tong, Y. Ren, T. Li, Y. Luo, N. Li, B. Tang, A. M. Asiri, M. S. Hamdy, Q. Kong, Z. Wang, X. Sun, Iron-doped cobalt oxide nanoarray for efficient electrocatalytic nitrate-to-ammonia conversion. *J. Colloid Interface Sci.*, 2022, **615**, 636-642.